
HOKKAIDO UNIVERSITY

| | |
|---|---|
| Title | Error-reduced channeled spectroscopic ellipsometer with palm-size sensing head |
| Author(s) | Okabe, Hiroshi; Hayakawa, Masayuki; Matoba, Junichi; Naito, Hitoshi; Oka, Kazuhiko |
| Citation | Review of Scientific Instruments, 80(8), 083104<br>https://doi.org/10.1063/1.3206346 |
| Issue Date | 2009-08 |
| Doc URL | http://hdl.handle.net/2115/39832 |
| Rights | Copyright 2009 American Institute of Physics. This article may be downloaded for personal use only. Any other use requires prior permission of the author and the American Institute of Physics. The following article appeared in Rev. Sci. Instrum. 80, 083104 (2009) and may be found at https://dx.doi.org/10.1063/1.3206346 |
| Type | article |
| File Information | RSI80-8_083104.pdf |


Instructions for use

Hokkaido University Collection of Scholarly and Academic Papers : HUSCAP

# Error-reduced channeled spectroscopic ellipsometer with palm-size sensing head

Hiroshi Okabe,[1,a)] Masayuki Hayakawa,[1] Junichi Matoba,[1] Hitoshi Naito,[1] and Kazuhiko Oka[2]
[1]*Core Technology Center, Omron Corporation, Kyoto 619-0283, Japan*
[2]*Division of Applied Physics, Graduate School of Engineering, Hokkaido University, Sapporo 060-8628, Japan*

(Received 31 March 2009; accepted 26 July 2009; published online 25 August 2009)

This paper describes a newly developed prototype system of the channeled spectroscopic ellipsometer (CSE). The new system has a feature that the major systematic and random error sources of the previous CSEs are effectively reduced or compensated for. In addition, the prototype preserves the advantageous features of the CSE in that it has a palm-size sensing head and that its acquisition time is as fast as 20 ms. Its performance is experimentally examined by use of 12 films whose thicknesses are ranging approximately from 3 to 4000 nm. The film thicknesses measured by the new CSE show good agreements with the ones by the rotating-compensator spectroscopic ellipsometer. The stability of the film-thickness measurement of the new CSE against the temperature change from 5 to 45 °C is less than 0.11 nm. The CSE can open up new applications of the spectroscopic ellipsometers in which the compactness, the simplicity, and the rapid response are important. © *2009 American Institute of Physics.* [DOI: 10.1063/1.3206346]

## I. INTRODUCTION

The channeled spectropolarimetry[1,2] is a snapshot method to measure the wavelength-resolved polarization of light or the dispersion characteristics of a polarimetric sample. The method utilizes high-order retarders whose retardations considerably vary with wavelength so that a finely and multiply modulated channeled spectrum is generated. This method has several remarkable features in that it requires neither mechanical nor active components for polarization control, such as a rotating compensator[3] and an electro-optic modulator,[4] and that multiple polarimetric parameters can be determined at once from a single channeled spectrum. In view of these features, the applications of the channeled spectropolarimetry have been extensively studied in various fields since the invention of its basic principle in 1998.[5–7] Among these works, the present authors have been developing the spectroscopic ellipsometer based on this method, called the channeled spectroscopic ellipsometer (CSE).[8]

The first CSE was designed with the analogy to the standard polarizer-sample-compensator-analyzer (PSCA) ellipsometer in 2000;[8,9] namely, the rotating compensator in the PSCA ellipsometer was substituted with two fixed high-order retarders, so that the state of polarization of the light reflected by a thin-film sample is measured by a channeled spectropolarimeter. Although the first CSE has a merit in that it is easy to understand its operational principle, it was quite susceptible to the fluctuation in the incident angle to the sample. To overcome this problem, the CSE with an alternative configuration was developed in 2005.[5] In the second CSE, the high-order retarders were moved from the receiving optics to the illumination optics so that the fluctuation due to the incident-angle variation can be effectively reduced. However, even the second CSE was not suited for the precise measurement of thin films, because some considerable errors due to unknown sources remained in the measured ellipsometric parameters by the second CSE.

To fully utilize the significant advantages of the channeled spectropolarimetry for the ellipsometric thin-film measurement, we have conducted error analysis for the previous CSEs. We consequently found several new error sources as well as the schemes to reduce them. Based on the results of the error analysis, the design of the CSE has been improved. In this paper, we will describe the new error-reduced CSE. It will be shown that, for measurements of the $SiO_2$ films whose thicknesses are ranging approximately from 3 to 4000 nm, the film thicknesses measured by the newly developed CSE are in good agreements with the ones by the commercially available rotating-compensator spectroscopic ellipsometer (RC-SE). Furthermore, the obtained film thicknesses of the three traceable samples were in good agreements with their certified values. We will also show that the newly developed CSE has good repeatability and stability and is almost immune to some external perturbations. The developed CSE has several advantageous features over the standard ellipsometer using rotating or electrically controlled polarimetric elements; for example, the CSE has a palm-size sensing head of 220 mm $(W)\times 45$ mm $(H)\times 30$ mm $(D)$, and the acquisition time is 20 ms. The reason why such a small sensing head and a short response time are easily realizable are that its configuration is simple and it requires neither mechanical nor active components for polarization control. In

a)Electronic mail: hiroshi_okabe@omron.co.jp.

 © 2009 American Institute of Physics

Downloaded 15 Nov 2009 to 133.87.26.227. Redistribution subject to AIP license or copyright; see http://rsi.aip.org/rsi/copyright.jsp

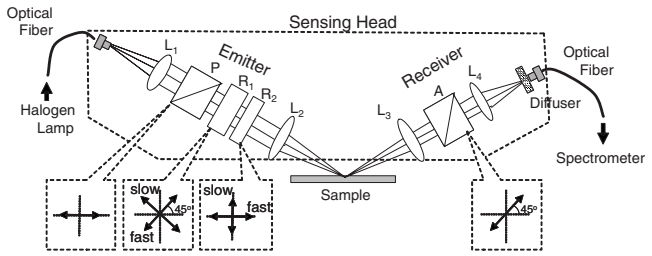


FIG. 1. Schematic diagram of the newly developed CSE.

view of these advantageous features, the CSE has a potential to open up new applications of the spectroscopic ellipsometers.

It should be noted that the features of the newly developed CSE was partly presented at a previous conference,[10] but the details of its design and the experiment, especially how the errors were reduced, were not described. We also note that all the previous reports about the CSEs appeared only in the conference proceedings,[5,8,10] and thus their descriptions about the principle only aimed for the particular studies. Accordingly, the formulations in the previous reports were not generalizable and especially not appropriate for the error analysis. In view of these circumstances, this paper also explains from the basic principle of the CSE so that we can derive the generalized formulation.

It should be also noted that a pioneering work about the use of the channeled spectrum for the ellipsometry was presented in 1983 by Yamamoto,[11] but its principle as well as objective are completely different from the present work. Yamamoto's ellipsometer is basically the null method using a rotating analyzer, by which the thickness of a thick film can be accurately determined. On the contrary, the CSE presented here aims to offer the snapshot method for the spectroscopic ellipsometry.

This paper is organized as follows. Section II describes the optical configuration as well as the basic features of the CSE and then derives the formulations of its principle. In Sec. III, the systematic errors of the previous CSE are explained, and the schemes to reduce them are introduced. Section IV is devoted to describe the techniques to enhance the stability against some external perturbations. The demonstration experiments and the discussions about the improved CSE is described in Sec. V.

## II. SYSTEM EXPLANATION

### A. Configuration of the channeled spectroscopic ellipsometer

The schematic diagram of the newly developed CSE is illustrated in Fig. 1. The major part of the CSE is the sensing head consisting of the emitter and receiver units. The respective units are connected to a halogen lamp and a spectrometer by use of multimode optical fibers. The sample is placed between the units so that the emitter and receiver units respectively serve as polarization state generator and analyzer.

The emitter unit includes a collimating lens $L_1$, a Glan–Taylor polarizer P, two high-order calcite retarders $R_1$ and $R_2$, and a condensing lens $L_2$. The transmission axis of P and the fast axis of $R_1$ intersect at 45° and the fast axis of $R_2$ is aligned to the transmission axis of P. The thicknesses of $R_1$ and $R_2$ are selected to be $D_1=450$ $\mu$m and $D_2=150$ $\mu$m. Note that the proper selection of these thicknesses is important to reduce the systematic error; the reason why we took the thickness ratio $D_1:D_2=3:1$ will be described in Sec. III A. The light from the halogen lamp passes though the emitter unit and then is incident onto the surface of a sample. The incident angle to the sample is 70°, and the diameter of the light spot at the sample is $1\times3$ mm$^2$.

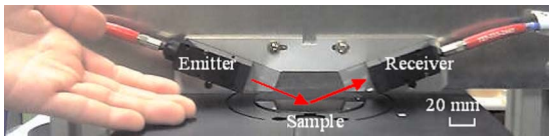


FIG. 2. (Color online) Photograph of the sensing head of the CSE.

The receiver unit includes a collimating lens $L_3$, a Glan–Taylor analyzer A, a condensing lens $L_4$, and a diffuser (a light shaping diffuser sheet, LSD 10°, Luminit, Torrance, CA). The transmission axis of A is oriented at 45° to the *p*-axis of the sample. The function of the diffuser will be described in Sec. IV A. The light reflected from the sample is collected by the receiver unit and then impinges upon a multichannel spectrometer through the optical fiber. The wavelength resolution of the spectrometer is 0.5 nm and its wavelength range is from $\lambda=500$ nm to $\lambda=850$ nm. It should be noted that fused-silica singlet lenses with a small numerical aperture (0.03) are used for the two lenses facing the sample, namely, $L_2$ and $L_3$, so that we can neglect their polarization imperfections.

Figure 2 shows the photograph of the fabricated sensing head. The size of the fabricated sensing head is 220 mm $(W)\times45$ mm $(H)\times30$ mm $(D)$; the sensing head is as small as the palm size as shown in the photograph. Such a small sensing head is realizable because its configuration is simple and it requires neither mechanical nor active components for polarization control. The fabricated system can acquire the channeled spectrum with an acquisition time of 20 ms, which determines the temporal resolution for the ellipsometric measurement.

Note that the set of optics consisting of a polarizer and two higher-order retarders, placed in the emitter unit, was named the channeled spectroscopic polarization state generator (CSPSG) in Ref. 12. On the other hand, the first CSE (Ref. 8) uses the channeled spectroscopic polarization state analyzer (CSPSA), consisting of two high-order retarders and an analyzer, in the receiving optics. It has been proved in our previous report[12] that the spectropolarimeter using the CSPSG (SP-CSPSG) is much less susceptible to the sample-induced fluctuations of the wavefront or ray direction than the spectropolarimeter using the CSPSA. This is the reason why the CSE of Fig. 1 is almost immune to the fluctuation in the incident angle to the sample.

### B. Basic operational principle of the channeled spectroscopic ellipsometer

We next describe the basic operational principle of the CSE. It should be first noted that the formulation in this subsection does not consider several error sources which

Downloaded 15 Nov 2009 to 133.87.26.227. Redistribution subject to AIP license or copyright; see http://rsi.aip.org/rsi/copyright.jsp

have been neglected in the previous studies of the CSE for the sake of the simplicity of the explanation. The effects of these error sources as well as the schemes to reduce them will be described in Sec. III.

Since the present configuration of the CSE can be interpreted as an application of the SP-CSPSG for the spectroscopic ellipsometry, we here follow the explanation in Ref. 12. The key devices of the SP-CSPSG are the high-order retarders, whose retardations considerably and almost linearly vary with the wavenumber $\sigma$, the reciprocal of the wavelength. Using $D_j$ $(j=1,2)$ for the thicknesses of $R_j$ and $B(\sigma)$ for their birefringence, the retardation $\phi_j(\sigma)$ of the high-order retarder $R_j$ can be written as[2]

$$\phi_j(\sigma) = 2\pi B(\sigma) D_j \sigma = 2\pi L_j \sigma + \Phi_j(\sigma). \tag{1}$$

Equation (1) shows that the retardation $\phi_j(\sigma)$ can be separated into the linear and nonlinear terms, defined as $2\pi L_j\sigma$ and $\Phi_j(\sigma)$, respectively. Provided that the dispersion of $B(\sigma)$ is considerably small, the variation of $\Phi_j(\sigma)$ is much smaller than that of the first term. This implies that $\phi_j(\sigma)$ varies almost linearly with $\sigma$.

With the variations of $\phi_1(\sigma)$ and $\phi_2(\sigma)$, the spectrum $P(\sigma)$ obtained from the spectrometer is finely modulated with the wavenumber; such a spectrum is called the channeled spectrum. The standard theory of the Muller calculus allows us to derive the formulation of the spectrum $P(\sigma)$. If we neglect the imperfections of the optical elements used in the CSE, $P(\sigma)$ is derived as[12]

$$\begin{aligned} P(\sigma) = {} & \tfrac{1}{2}P_0(\sigma)m_{00}(\sigma) + \tfrac{1}{2}P_0(\sigma)m_{01}(\sigma)\cos\,\phi_1(\sigma) \\ & + \tfrac{1}{4}P_0(\sigma)|m_{0(23)}(\sigma)|\cos[\phi_1(\sigma) - \phi_2(\sigma) \\ & \qquad + \arg\{m_{0(23)}(\sigma)\}] \\ & - \tfrac{1}{4}P_0(\sigma)|m_{0(23)}(\sigma)|\cos[\phi_1(\sigma) + \phi_2(\sigma) \\ & \qquad - \arg\{m_{0(23)}(\sigma)\}], \end{aligned} \tag{2}$$

with

$$m_{00}(\sigma) = 1/2, \tag{3a}$$

$$m_{01}(\sigma) = -(1/2)\cos 2\Psi(\sigma), \tag{3b}$$

$$m_{0(23)}(\sigma) = m_{02}(\sigma) - im_{03}(\sigma), \tag{3c}$$

$$m_{02}(\sigma) = (1/2)\sin 2\Psi(\sigma)\cos\Delta(\sigma), \tag{3d}$$

$$m_{03}(\sigma) = (1/2)\sin 2\Psi(\sigma)\sin\Delta(\sigma), \tag{3e}$$

where $P_o(\sigma)$ is the spectrum of the light source and $\Psi(\sigma)$ and $\Delta(\sigma)$ are the wavenumber-dependent ellipsometric parameters of the sample. Equations (1) and (2) imply that $P(\sigma)$ is composed of one slowly varying component and three quasicosinusoidal components whose carrier frequencies are $L_1$, $L_-(=L_1-L_2)$, and $L_+(=L_1+L_2)$, respectively. These components carry the information about either $m_{01}(\sigma)$ or $m_{0(23)}(\sigma)$. Note that $m_{0k}(\sigma)$ $(k=0,\ldots,3)$ are the four elements in the first row of the Muller matrix of a block consisting of the sample and the analyzer.[12]

Fourier analysis of $P(\sigma)$ allows us to demodulate $m_{0k}(\sigma)$ separately from the spectrum provided that the retardations $\phi_1(\sigma)$ and $\phi_2(\sigma)$ are calibrated in advance. The ellipsometric parameters of the sample can now be determined from $m_{0k}(\sigma)$ as

$$\Psi(\sigma) = -\tan^{-1}\frac{\sqrt{m_{02}^2(\sigma) + m_{03}^2(\sigma)}}{m_{01}(\sigma)}, \tag{4a}$$

$$\Delta(\sigma) = \tan^{-1}\frac{m_{03}(\sigma)}{m_{02}(\sigma)}. \tag{4b}$$

Consequently, we can obtain both $\Psi(\sigma)$ and $\Delta(\sigma)$ simultaneously and independently only from a single channeled spectrum $P(\sigma)$. In other words, the snapshot measurement of both $\Psi(\sigma)$ and $\Delta(\sigma)$ can be realized with the CSE.

## III. REDUCTION OF SYSTEMATIC ERRORS

In the early studies of the CSE,[5] the simple theory described in Sec. II B was used as it is for the measurement of the ellipsometric parameters. However, it has been soon recognized that the theory was inappropriate for the precise ellipsometric measurements because several imperfections of the system causing systematic errors were neglected. We then analyzed the characteristics of the imperfections to reduce the errors. In this section, we describe the error sources of the previous CSEs and the schemes to reduce their effects.

### A. Polarization-dependent Fresnel reflections of high-order retarders

The high-order retarders of the palm-size CSE are made of calcite because it is the highly birefringent material and thus appropriate for the reduction of the sensing-head size. However, the calcite retarders have a drawback in that the transmittances for the fast and slow components are different from each other. This is because the Fresnel reflectances at the input and output faces of the retarder depend on the refractive index of the retarder material and thus vary with the polarization direction, even though the diattenuation of the material itself is almost negligible. It turns out that this effect is one of the major error sources for the CSE.

From now on, we will revise Eq. (2) to include the effects from the polarization dependent Fresnel reflectances of the retarders. Let $T_s(\sigma)$ and $T_f(\sigma)$ be the transmittances for the slow and fast axes of the retarder. We here introduce the transmittance ratio angle $\gamma(\sigma)=\tan^{-1}[T_s(\sigma)/T_f(\sigma)]$. As a numerical example, the ordinary and extraordinary refractive indices of calcite at $\lambda=589$ nm $(\sigma=1.70\times10^4\ \mathrm{cm}^{-1})$ are 1.6548 and 1.4864,[13] and thereby $\gamma(1.70\times10^4\ \mathrm{cm}^{-1}) = 44.320°$. Provided that the $\gamma(\sigma)$ of $R_1$ and $R_2$ are the same, the spectrum $P(\sigma)$ is revised to include $\gamma(\sigma)$ as

$$\begin{aligned} P(\sigma) = {} & \tfrac{1}{2}P_0(\sigma)[m_{00}(\sigma) + \cos 2\gamma(\sigma)m_{01}(\sigma)] \\ & + \tfrac{1}{2}\sin 2\gamma(\sigma)P_0(\sigma)[m_{01}(\sigma) \\ & \qquad + \cos 2\gamma(\sigma)m_{00}(\sigma)]\cos\,\phi_1(\sigma) \\ & + \tfrac{1}{4}\sin^2 2\gamma(\sigma)P_0(\sigma)|m_{23}(\sigma)|\cos[\phi_1(\sigma) - \phi_2(\sigma) \\ & \qquad + \arg\{m_{23}(\sigma)\}] \\ & - \tfrac{1}{4}\sin^2 2\gamma(\sigma)P_0(\sigma)|m_{23}(\sigma)|\cos[\phi_1(\sigma) + \phi_2(\sigma) \end{aligned}$$

Downloaded 15 Nov 2009 to 133.87.26.227. Redistribution subject to AIP license or copyright; see http://rsi.aip.org/rsi/copyright.jsp

$$- \arg\{m_{23}(\sigma)\}]$$
$$- \tfrac{1}{4}\sin 4\gamma(\sigma)P_0(\sigma)|m_{23}(\sigma)|\cos[\phi_2(\sigma) - \arg\{m_{23}(\sigma)\}]. \quad (5)$$

Comparing Eq. (5) with Eq. (2), we can see that the unbalanced Fresnel reflections of the high-order retarders cause the following changes to the obtained channeled spectrum.

- The fifth term in Eq. (5) is added to $P(\sigma)$ from Eq. (2). Since $\phi_2(\sigma)$ is almost linearly related to $\sigma$ as $2\pi L_2\sigma$, the added term is also quasicosinusoidal but has a central (carrier) frequency of $L_2$.
- The first and second terms in Eq. (5) become dependent upon both $m_{00}$ and $m_{01}$. The corresponding terms in Eq. (2), in which the effect of the Fresnel reflection was not considered, were only related to either $m_{00}$ or $m_{01}$.
- Amplitude coefficients of all quasicosinusoidal components become dependent on $\gamma(\sigma)$.

As will be experimentally shown in Sec. V A, the neglect of the unbalanced Fresnel reflection effect was one of the major error sources of the previous CSE. To solve this problem, we modified the optical arrangement and improved the demodulation scheme.

The first effect can be eliminated by altering the thickness ratio of the high- order retarders $R_1$ and $R_2$ from $D_1:D_2=2:1$ to 3:1. To understand the reason for this change, we now examine the Fourier inversion of $P(\sigma)$, namely, the autocorrelation function $C(h)$. If the unbalanced Fresnel reflections of the retarders were neglected, the thickness ratio of 2:1 would be the optimum,[14] because the seven correlational components in $C(h)$, whose carrier frequencies derived from Eq. (2) are $h=0$, $\pm L_-$, $\pm L_1$, and $\pm L_+$, would be equally spaced over the $h$-axis, as shown in Fig. 3(a). Unfortunately, however, the unbalanced Fresnel reflections cannot be neglected with the calcite retarders, and thereby the emerging components at $h=\pm L_2$ overlap with $\pm L_-$ components in the previous CSE employing the ratio 2:1, as shown in Fig. 3(b). Accordingly, we altered the thickness ratio to $D_1:D_2=3:1$ with the new CSE, as the nine components, including $\pm L_2$ components, are equally spaced over the $h$-axis as shown in Fig. 3(c).

Note that the presence of the $L_2$ component in the channeled spectrum has been pointed out in some previous studies of the channeled spectropolarimetry, but they were the cases such that the polarization axes are misaligned and that the retarder material has big diattenuation.[7,15] However, the discussion here shows that, even when we use perfectly aligned retarders with no diattenuation, the $L_2$ component cannot be eliminated when we use the calcite retarders.

The other error sources, namely, the second and third factors in the above list, can be avoided by slightly modifying the signal processing scheme. As for the second factor causing the cross coupling between $m_{00}(\sigma)$ and $m_{01}(\sigma)$, its effect can be compensated for by solving the simultaneous equations between the coefficients of the components at $h=0$ and $L_1$. In addition, the unwanted effects due to the third factor can be compensated for by considering $\gamma(\sigma)$. Note that $\gamma(\sigma)$ must be obtained in advance to the compensation; they can be easily obtained by the calibration or the calculation from the Sellmeier equations.

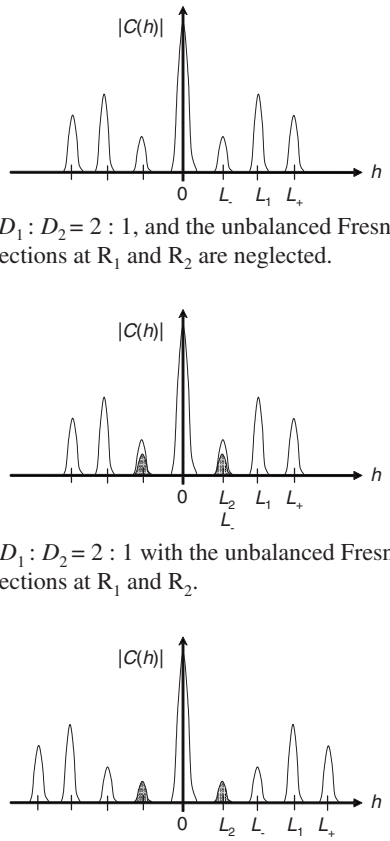


(a) $D_1:D_2=2:1$, and the unbalanced Fresnel reflections at $R_1$ and $R_2$ are neglected.

(b) $D_1:D_2=2:1$ with the unbalanced Fresnel reflections at $R_1$ and $R_2$.

(c) $D_1:D_2=3:1$ with the unbalanced Fresnel reflections at $R_1$ and $R_2$.

FIG. 3. Schematics of the autocorrelation function $C(h)$ under various conditions.

### B. Bandwidth limitation during the demodulation of the ellipsometric parameters

Another major systematic error source for the CSE is the bandwidth limitation induced by the filtering operation during the demodulation of the ellipsometric parameters. As has been described in Sec. II B, the modulations $m_{0k}(\sigma)$ $(k=0,\ldots,3)$ for the respective quasicosinusoidal components are demodulated from $P(\sigma)$ by use of the Fourier analysis. Specifically, at first $P(\sigma)$ is Fourier inverse transformed to give the autocorrelation function $C(h)$ of Fig. 3(c), and then the respective components are filtered out to give $m_{0k}(\sigma)$. In this demodulation, the filtering operation introduces the bandwidth limitation to $m_{0k}(\sigma)$. This limitation brings about considerable errors in the computed ellipsometric parameters.

The bandwidth-limitation effect can be formulated by use of the convolution integral, similar to the frequency filtering in the field of the electronic communications. Using $w(\sigma)$ for the Fourier transformation of the filtering function to extract the modulations of the respective quasicosinusoidal components, the demodulated modulations can be expressed as

Downloaded 15 Nov 2009 to 133.87.26.227. Redistribution subject to AIP license or copyright; see http://rsi.aip.org/rsi/copyright.jsp

$$m'_{01}(\sigma) = m_{01}(\sigma) * w(\sigma) = -(1/2)\cos 2\Psi(\sigma) * w(\sigma), \tag{6a}$$

$$m'_{0(23)}(\sigma) = \{m_{02}(\sigma) - im_{03}(\sigma)\} * w(\sigma)$$

$$= (1/2)\{\sin 2\Psi(\sigma)\cos \Delta(\sigma) - i \sin 2\Psi(\sigma)\sin \Delta(\sigma)\} * w(\sigma), \tag{6b}$$

where $*$ denotes the operator for the convolution integral. We here assumed that the variations of $\Phi_1(\sigma)$, $\Phi_2(\sigma)$, and $P_0(\sigma)$ can be neglected within the width of $w(\sigma)$. Note that the detailed derivation and analysis of the above equations will be discussed elsewhere. With reference to Eqs. (4a), (4b), (6a), and (6b), the ellipsometric parameters demodulated from the bandwidth-limited modulations $m'_{01}(\sigma)$ and $m'_{0(23)}(\sigma)$ take the forms as

$$\Psi'(\sigma) = -\tan^{-1}[|\{\sin 2\Psi(\sigma)\cos \Delta(\sigma) - i \sin 2\Psi(\sigma)\sin \Delta(\sigma)\} * w(\sigma)|/[\{\cos 2\Psi(\sigma)\} * w(\sigma)]], \tag{7a}$$

$$\Delta'(\sigma) = \arg[\{\sin 2\Psi(\sigma)\cos \Delta(\sigma) - i \sin 2\Psi(\sigma)\sin \Delta(\sigma)\} * w(\sigma)], \tag{7b}$$

where arg stands for the operator to take the argument of the complex value. Therefore, the bandwidth limitation during the demodulation using the Fourier transformation affects the demodulated ellipsometric parameters.

Fortunately, in most of the ellipsometric studies, the effect of this bandwidth limitation can be reduced by the modification of the signal processing algorithm. We here note that the objective of the ellipsometric measurements are usually not to obtain the ellipsometric parameters themselves but to determine the other geometrical or material parameters of the sample, such as the film thicknesses and the dielectric constants. For this purpose, the numerical fitting between the experimentally measured and theoretically computed ellipsometric parameters are employed in most of the ellipsometric studies of thin films. This implies that the effect of the bandwidth limitation can be reduced by including Eqs. (7a) and (7b) in the theoretical model for the numerical fitting.

It will be experimentally shown in Sec. V A that this modified fitting algorithm is especially significant for a sample with a thick film. We here note that we can use various types of standard window functions for $w(\sigma)$, because its variation can be compensated for with the algorithm described above. With our prototype of the CSE, we used the Hanning window function in the $h$-domain to extract the components from $C(h)$. In this case, $w(\sigma)$ is its Fourier transformation,

$$w(\sigma) = \frac{L_2}{2}\frac{\mathrm{sinc}(L_2\sigma)}{1 - L_2^2\sigma^2}, \tag{8}$$

where $\mathrm{sinc}(x) = \sin(\pi x)/(\pi x)$.

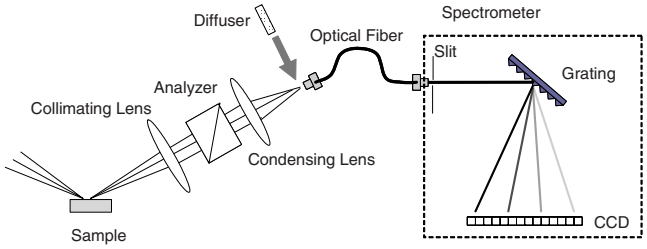


FIG. 4. (Color online) Schematic illustrating the part of the optical system from the sample to the spectrometer. The fluctuations in the measured ellipsometric parameters due to the fiber bending can be effectively reduced by inserting a diffuser in front of the optical fiber.

## IV. ENHANCEMENT OF STABILITY AGAINST EXTERNAL PERTURBATIONS

For the precise measurement of the CSE, we need to decrease not only the systematic, namely, repeatable errors, but also the random errors caused by the external perturbations. In this section, we discuss the sources of the instability and also describe the schemes to eliminate their effects. We have found that there are two major causes of the random errors with the CSE; one is the instability of the optical fibers and the other is the temperature dependence of the high-order retarders.

### A. Perturbation due to bending of optical fiber

In the fabricated palm-size CSE, two multimode optical fibers are used for the connections among the light source, the sensing head, and the spectrometer. It is essential to use the fibers for the miniaturization of the sensing head of the CSE, as has been described in Sec. II A. However, we experimentally found that the measured values of our fabricated CSE were easily altered with the external stimulations to one of the fibers, the one connecting the receiver unit to the spectrometer. Note that the measured data were almost immune to the stimulation to the other fiber.

The reason of the above instability can be explained by considering the intensity distribution over the entrance slit in the spectrometer. Figure 4 illustrates the optical system of the part of the CSE from the sample to the spectrometer. When the diffuser is not present as was in the previous system, only some low-order modes are excited within the fiber, and hence the spatial intensity distribution over the output face of the multimode optical fiber is not homogeneous. In this case, the output spatial intensity distribution drastically changes with the external perturbations to the fiber, such as the random bent, because the random mode coupling takes place within the fiber. This implies that the obtained spectrum also varies with the fluctuation of the fiber.

To minimize the error related to the fluctuation of the fiber, we introduce a diffuser in front of the fiber with the new prototype system. The diffuser excites much more modes in the fiber, including many higher modes. Since higher modes have considerably different phase velocities from the ones of the lower modes, the beam emerging from the fiber, which is the superposition of the many modes, has spatially homogeneous intensity distribution and becomes almost perfectly spatially incoherent. Furthermore, the inten-

Downloaded 15 Nov 2009 to 133.87.26.227. Redistribution subject to AIP license or copyright; see http://rsi.aip.org/rsi/copyright.jsp

sity is much less susceptible to the change of the mode coupling because of the intensity averaging among the many modes. As a result, the incorporation of the diffuser allows us to minimize the error due to the bending of the optical fiber.

### B. Temperature dependence of high-order retarders

The reason why the previous CSE was susceptible to the temperature change is that it uses the high-order retarders. Since the thicknesses of the high-order retarders are much larger than those of the usual zero-order retarders, the retardations $\phi_1(\sigma)$ and $\phi_2(\sigma)$ of the high-order retarders considerably change with the temperature. Although these retardations usually are calibrated in advance to the measurements, the temperature can vary during the time interval between the calibration and the measurement, and thereby the temperature change introduces the considerable error in the measured ellipsometric parameters. To overcome this drawback, we employ the self-calibration technique.[16] Since the technique was originally developed for use with the CSPSA, we modified it for use with the CSE.

To describe the principle of the self-calibration technique for the CSE, we here decompose $\phi_j(\sigma)$ $(j=1,2)$ as

$$\phi_j(\sigma) = \phi_j^{(i)}(\sigma) + \delta\phi_j(\sigma), \tag{9}$$

where $\phi_j^{(i)}(\sigma)$ is the phase retardation at the time of the calibration, and $\delta\phi_j(\sigma)$ is the deviation between the calibration and the measurement. Using $\phi_j^{(i)}(\sigma)$ and $\delta\phi_j(\sigma)$, the complex components with the carrier frequencies of $L_1$, $L_-$, and $L_+$ demodulated from $P(\sigma)$ are expressed as

$$F_1(\sigma) = K_1^{(i)}(\sigma)e^{i\delta\phi_1(\sigma)}P_0(\sigma)[m_{01}(\sigma) + \cos 2\gamma(\sigma)m_{00}(\sigma)], \tag{10a}$$

$$F_-(\sigma) = K_-^{(i)}(\sigma)e^{i\{\delta\phi_1(\sigma)-\delta\phi_2(\sigma)\}}P_0(\sigma)m_{0(23)}(\sigma), \tag{10b}$$

$$F_+(\sigma) = K_+^{(i)}(\sigma)e^{i\{\delta\phi_1(\sigma)+\delta\phi_2(\sigma)\}}P_0(\sigma)m_{0(23)}^*(\sigma), \tag{10c}$$

where

$$K_1^{(i)}(\sigma) = 1/4 \sin 2\gamma(\sigma)e^{i\phi_1^{(i)}(\sigma)}, \tag{11a}$$

$$K_-^{(i)}(\sigma) = 1/8 \sin^2 2\gamma(\sigma)e^{i\{\phi_1^{(i)}(\sigma)-\phi_2^{(i)}(\sigma)\}}, \tag{11b}$$

$$K_+^{(i)}(\sigma) = -1/8 \sin^2 2\gamma(\sigma)e^{i\{\phi_1^{(i)}(\sigma)+\phi_2^{(i)}(\sigma)\}}. \tag{11c}$$

From Eqs. (10) and (11), we obtain

$$\delta\phi_1(\sigma) = \frac{1}{2}\tan^{-1}\left\{\left[\frac{F_1(\sigma)}{K_1^{(i)}(\sigma)}\right]^2 + \frac{F_-(\sigma)F_+(\sigma)}{K_-^{(i)}(\sigma)K_+^{(i)}(\sigma)}\right\}. \tag{12}$$

The right hand side of Eq. (12) includes only the measurable values. Specifically, $F_1(\sigma)$, $F_-(\sigma)$, and $F_+(\sigma)$ can be demodulated from $P(\sigma)$ by use of the Fourier transform method.[2,16] On the other hand, $K_1^{(i)}(\sigma)$, $K_-^{(i)}(\sigma)$, and $K_+^{(i)}(\sigma)$ can be calibrated in advance to the measurement, since they only include the parameters independent of both the sample and the retardation variations. This implies that we can compute $\delta\phi_1(\sigma)$ from the channeled spectrum $P(\sigma)$ even when an unknown sample is placed. The variation of the retardation of the other retarder can be obtained from $\delta\phi_1(\sigma)$ as

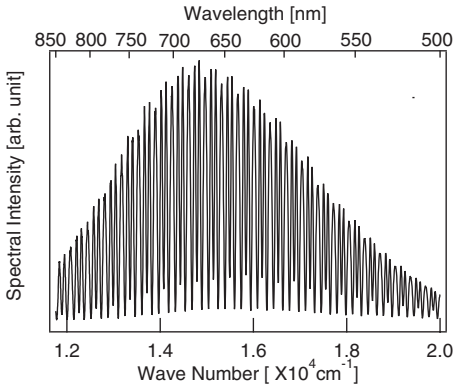


FIG. 5. Channeled spectrum $P(\sigma)$ measured with sample C.

$\delta\phi_2(\sigma) = (D_2/D_1)\delta\phi_1(\sigma)$. Therefore, we can compensate for the phase retardations of both $R_1$ and $R_2$ using $\delta\phi_1(\sigma)$ and $\delta\phi_2(\sigma)$.

The self-calibration technique described here allows us to compensate for the variations in $\phi_1(\sigma)$ and $\phi_2(\sigma)$ during the measurement of the ellipsometric parameters. In addition, the technique requires any additional instruments, such as a temperature monitor or a temperature controller. This implies that the compensations of the phase retardations can be made without sacrificing the major merits of the CSE, namely, the simplicity and the compactness of the optical system.

## V. EXPERIMENTAL DEMONSTRATION AND DISCUSSION

### A. Accuracy and repeatability of $SiO_2$ film-thickness measurements

The performance of the fabricated prototype of the CSE was experimentally examined. Twelve different $SiO_2$ films on Si substrates, respectively designated by samples A–L, were supplied for the experiment. Their thicknesses are ranging approximately from 3 to 4000 nm. For comparison, the commercially available RC-SE was also used to measure the same samples. Note that sample A is a reference thin-film material supplied from National Metrology Institute of Japan (NMIJ), and samples B and C are the reference materials supplied from National Institute of Standards Technology (NIST), USA. The certified values of samples A, B, and C are $3.49 \pm 0.19$, $8.80 \pm 0.4$, and $48.5 \pm 0.6$ nm, respectively.

In what follows, we will show the thickness-measurement results by use of the CSE. In Sec. V A 1, we confine ourselves to the experiment with a thin-film sample (sample C). We will see that the technique described in Sec. III A is inevitable for the accurate measurements of thin films by the CSE. In Sec. V A 2, the experiment with a fairly thick sample (sample J) is described. It will be shown that the modified numerical fitting scheme of Sec. III B is effective for the thick-film sample. In Sec. V A 3, the accuracy and the repeatability for the measurement of all the 12 samples are explained.

#### *1. Measurement with a thin-film sample (sample C)*

The channeled spectrum $P(\sigma)$ obtained with sample C is shown in Fig. 5. The finely modulated spectrum carries the

Downloaded 15 Nov 2009 to 133.87.26.227. Redistribution subject to AIP license or copyright; see http://rsi.aip.org/rsi/copyright.jsp

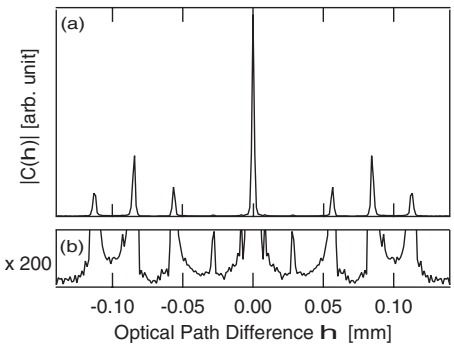


FIG. 6. Absolute value of the autocorrelation function $|C(h)|$ calculated from Fig. 5. The vertical-axis scale of (b) is expanded by 200 times from that of (a).

information of both ellipsometric parameters $\Psi(\sigma)$ and $\Delta(\sigma)$ of the thin-film sample. The Fourier inversion of $P(\sigma)$ immediately gives the autocorrelation function $C(h)$ of the light incident on the spectrometer, where $h$ stands for the optical path difference. Its absolute value $|C(h)|$ is plotted in Fig. 6. In this figure, (a) and (b) show the same correlation function, but the scale of the vertical axis of (b) is expanded by 200 times from that of (a). These figures show that $C(h)$ includes not only seven apparent peaks, respectively centered at $h=0$ mm, $\pm L_{-}(\pm 0.057$ mm), $\pm L_1(\pm 0.085$ mm), and $\pm L_{+}(\pm 0.113$ mm), but also two weak peaks centered at $\pm L_2(\pm 0.028$ mm). The two weak peaks result from the polarization-dependent Fresnel reflection at the high-order retarders, as discussed in Sec. II A. As shown in Fig. 6, all the peak components are successively separated one another over the $h$-axis, even with the presence of the weak peaks at $\pm L_2$.

The spectrally resolved ellipsometric parameters $\Delta(\sigma)$ and $\Psi(\sigma)$ were demodulated from the autocorrelation function $C(h)$; the obtained values are plotted by the solid lines in Fig. 7. These ellipsometric parameters were then numerically fitted with a theoretical model to show the effectiveness of the CSE. Note that two different procedures for the numerical fitting were employed with the identical ellipsometric parameters of Fig. 7; the first procedure varies only the thickness of the $SiO_2$ film for the fitting, whereas both the thickness and refractive index of the film are varied in the second fitting procedure.

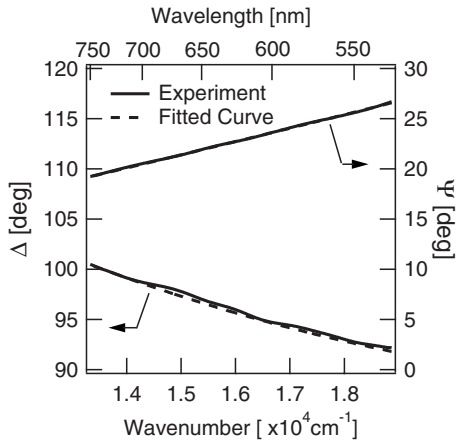


FIG. 7. Ellipsometric parameters $\Psi(\sigma)$ and $\Delta(\sigma)$ of sample C. Solid lines were experimentally obtained from the CSE, whereas dashed lines show the numerically fitted results by the first procedure.

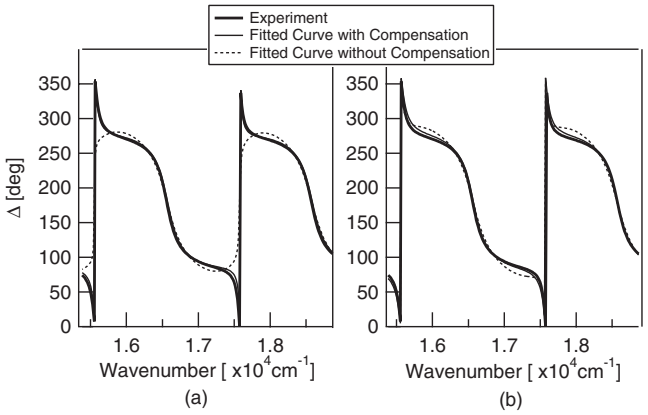


FIG. 8. Experimentally obtained and numerically fitted ellipsometric parameters $\Delta(\sigma)$ of sample J. Thick-solid line is for the experimentally obtained value, and the thin-solid and broken lines are the fitted curves obtained with and without the compensation based on Eqs. (7a) and (7b). (a) is obtained when the film thickness is only varied for the fitting, and (b) is obtained when both the thickness and the refractive index of the film are varied.

In the first procedure, the refractive indices of Si substrate and $SiO_2$ film were fixed to the tabulated data in Ref. 17, and only the film thickness was varied so that the mean square error becomes minimum.[18] The resultant fitted curves are shown by the broken lines in Fig. 7. The film thickness derived from this fitting is 48.90 nm. For comparison, the film thickness was also measured by the RC-SE; the measured value is 48.87 nm. The thicknesses measured by the CSE and the RC-SE are almost coincide with each other and also show good agreement with the NIST certified value, $48.5 \pm 0.6$ nm.

In the second procedure, two-term Cauchy expression with no absorption, according to the formulas $n(\sigma)=A+B\sigma^2$, were used for the refractive index of the film, where two Cauchy coefficients, $A$ and $B$, were varied as the fitting parameters together with the film thickness. As the result of the fitting, the film thickness is estimated to be 49.18 nm, whereas the Cauchy coefficients are obtained as $A=1.444$ and $B=0.0028$. The refractive index at wavelength of 600 nm calculated from the obtained Cauchy coefficients is 1.451, which is in good agreement with the reference value, 1.458.[17]

We now discuss about the necessity to take the 3:1 thickness ratio for the retarders. For this purpose, we first recall the previous experiment by the second prototype of the CSE whose retarders took the thickness ratio of 2:1.[5] In the experiment, a sample similar to sample C was measured by the previous CSE as well as the RC-SE. The obtained thicknesses of the sample by the previous CSE and RC-SE were 52.6 and 49.3 nm, respectively, and then the difference between them was 3.3 nm. In contrast, the new CSE having the 3:1 thickness ratio offers closer result to that by the RC-SE. For example, the difference between the thicknesses of sample C measured by the new CSE with the first procedure and by the RC-SE is only 0.03 nm. This fact implies that the inappropriate selection of the thickness ratio of the retarders

Downloaded 15 Nov 2009 to 133.87.26.227. Redistribution subject to AIP license or copyright; see http://rsi.aip.org/rsi/copyright.jsp

was the major error source of the previous CSE. In fact, as has been shown in Fig. 6, the channeled spectrum of the new CSE includes weak peaks at $\pm L_2$ which is mainly induced by the unbalanced Fresnel reflections at the retarders. If we took the 2:1 ratio, these peaks overlapped with the necessary components at $L_-$ and thus we could not eliminate them from the channeled spectrum. On the contrary, as has been described in Sec. III A, the peaks at $\pm L_2$ do not overlap with those at $\pm L_-$ with the thickness ratio of 3:1, and thus they do not affect the measured ellipsometric parameters. Consequently, the error of the first CSE should mainly be caused by the unbalanced Fresnel reflection effect and its effect can be effectively reduced by taking the thickness ratio of 3:1.

#### 2. Measurement with a thick-film sample (sample J)

We next show the results with sample J whose film thickness is approximately 2000 nm. The ellipsometric parameters of such a fairly thick film considerably vary with the wavelength, and hence the measured ellipsometric parameters are affected by the bandwidth-limitation effect discussed in Sec. III B.

In the same manner with the thin-film sample C described in Sec. V A 1, two fitting procedures with different variable parameters were employed with the measured ellipsometric parameters of sample J. In both procedures, the theoretical models without and with considering Eqs. (7a) and (7b) are alternatively used to show the feasibility of the compensation described in Sec. III B.

Figure 8(a) shows the results with the first fitting procedure in which only the film thickness of $SiO_2$ is varied as a fitting parameter. In this figure, the thick-solid line is $\Delta(\sigma)$ measured by the CSE, and the thin-solid and broken lines are the fitting curves with and without the compensation based on Eqs. (7a) and (7b), respectively. The curve fitted with the compensation almost overlaps with the experimental curve, whereas the one obtained without the compensation shows apparent discrepancy around the wavelength where $\Delta(\sigma)$ drastically varies. However, the film thicknesses obtained by both fittings with and without the compensation were of the same value, 2167 nm. It is a somewhat strange result because it seems to show that the compensation is not necessary when the thickness is the only parameter to be determined. Nevertheless Fig. 8(a) shows clear advantage of the fitting with the compensation.

The results by the second numerical fitting procedure, in which both the thickness and the refractive index of $SiO_2$ film are varied, is shown in Fig. 8(b) and Table I; Fig. 8(b) is the dispersion curves of the experimentally obtained and numerically fitted $\Delta(\sigma)$, and Table I shows obtained values for the film thickness, the Cauchy coefficients $A$ and $B$, and the refractive index at 600 nm. Similar to Fig. 8(a), the fitted curve with the compensation well overlaps with the experimental curve, whereas the fitted curve without the compensation does not agree with it. However, the discrepancy between the curves with and without the compensation decreases from Fig. 8(a). On the other hand, the parameters in Table I, obtained with and without the compensation, shows a clear difference. From the comparison with the results by the first procedure described in the previous paragraph, we see that the film thickness obtained by the first procedure (2167 nm) is much closer to the one obtained by the second procedure with the compensation (2153 nm) than to that without the compensation (2045 nm). Furthermore, the reference value of the refractive index at 600 nm (1.458) is also much closer to the value obtained with the compensation (1.464) than to the value obtained without compensation (1.510). The above results show the effectiveness of the compensation based on Eqs. (7a) and (7b), especially for the fairly thick samples.

TABLE I. Results of the numerical fitting by the second procedure in which both the thickness and refractive index of the film are varied as the fitting parameters. The upper and lower rows are respectively obtained without and with the compensation based on Eqs. (7a) and (7b). The refractive indices at 600 nm are calculated from $A$ and $B$.

| Theoretical model | Thickness (nm) | Refractive index | | |
|---|---|---|---|---|
| | | $A$ | $B$ | At 600 nm |
| Without compensation | 2045 | 1.496 | 0.0048 | 1.510 |
| With compensation | 2153 | 1.452 | 0.0043 | 1.464 |

#### 3. Measurements with 12 samples

For the 12 $SiO_2$ films with a variety of thicknesses, the film thicknesses were measured by both the CSE and the RC-SE. The obtained values are shown in Table II. It is shown that all of the film thicknesses obtained by the CSE agree well with the ones by the RC-SE. Furthermore, the measured film thicknesses of the three traceable samples A–C are in good agreement with their certified values.

To show the static repeatability, 20 replicate measurements at the same spot location by the CSE were made; the standard deviations of the measurements are shown in Table III. The standard deviations are less than 0.03 nm, except for samples K and L which are thicker than 3000 nm. These

TABLE II. Measured film thicknesses of 12 different $SiO_2$ films.

| | Sample | | | | | | | | | | | |
|---|---|---|---|---|---|---|---|---|---|---|---|---|
| | A[a] | B[b] | C[c] | D | E | F | G | H | I | J | K | L |
| CSE (nm) | 3.68 | 9.30 | 48.90 | 84.86 | 181.8 | 288.4 | 392.5 | 499.5 | 1034 | 2167 | 3054 | 4103 |
| RC-SE (nm) | 3.70 | 9.09 | 48.87 | 84.80 | 182.4 | 288.1 | 392.4 | 499.8 | 1033 | 2165 | 3041 | 4131 |

[a]NMIJ traceable sample. Certified value is $3.49 \pm 0.19$.
[b]NIST traceable sample. Certified value is $8.80 \pm 0.4$.
[c]NIST traceable sample. Certified value is $48.5 \pm 0.6$.

Downloaded 15 Nov 2009 to 133.87.26.227. Redistribution subject to AIP license or copyright; see http://rsi.aip.org/rsi/copyright.jsp

TABLE III. Repeatability of the CSE in the film-thickness measurement. Each value shows the standard deviation of the measured thicknesses which is calculated from the results of 20 replicate measurements at the same spot location of a sample.

| | Sample | | | | | | | | | | | |
|---|---|---|---|---|---|---|---|---|---|---|---|---|
| | A | B | C | D | E | F | G | H | I | J | K | L |
| $\sigma$ (nm) | 0.03 | 0.02 | 0.03 | 0.01 | 0.01 | 0.02 | 0.02 | 0.02 | 0.02 | 0.03 | 0.07 | 0.08 |

results demonstrate that the CSE has good accuracy and repeatability sufficient for some applications of the film-thickness measurement.

### B. Stability against the external perturbations

We next show the stability of the CSE against some external perturbations. Note that the samples used in this subsection are different from samples A–L used in Sec. V A because of the convenience for the experiment.

#### *1. Stability against optical fiber bending*

To examine the stability against the stimulations to the optical fiber, the thickness measurement of a $SiO_2$ film was repeated with the random bending of the optical fiber. Following the discussion in Sec. IV A, the experiment was conducted for both the cases without and with a diffuser and almost the same fiber bending was applied to both cases. The core diameter of the each optical fiber is 1 mm and its length is 2 m.

Figure 9 shows the variations of the ellipsometric parameter $\Delta(\sigma)$; (a) and (b) were respectively taken without and with using the diffuser. They were obtained from 20 replicate measurements of a sample under the condition that the receiver's optical fiber was randomly bended. It is clearly shown that the case with the diffuser is much less susceptible to the fiber bending than the case without the diffuser. The means and the standard deviations of the measured film thicknesses were $48.10 \pm 0.17$ and $48.06 \pm 0.03$ nm, respectively, for (a) and (b). Note that the standard deviation of the case with the diffuser is almost the same with that in Table III whose data were taken under no fluctuation to the fibers. This implies that the perturbation due to the fiber bending can be almost completely suppressed by the incorporation of the diffuser.

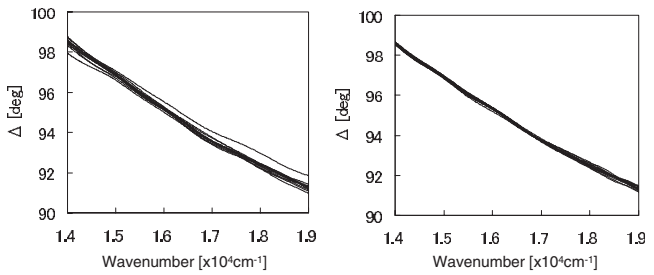


(a) Without Diffuser (WOD) (b) With Diffuser (WD)

FIG. 9. Fluctuations of the measured ellipsometric parameter $\Delta(\sigma)$ under fiber bending. (a) and (b) are respectively taken without and with using a diffuser.

#### *2. Stability against temperature change*

The feasibility of the self-calibration technique against the temperature change was examined by use of a temperature controlled bath; the experimental system including both the CSE and the sample is placed into the bath, and the thickness measurement was repeated by changing the ambient temperature from 5 to 45 °C.

Three $SiO_2$ films on Si substrates whose thicknesses are different from one another were supplied for the experiment. The film thicknesses measured by the CSE at the temperature of 25 °C are 2.28, 7.46, and 53.77 nm, respectively.

Figure 10 shows the shifts in the measured thicknesses with the temperature change. In this figure, the shifts were plotted with reference to the measured values at 25 °C. (a) and (b) of the figure respectively show the results obtained without and with the self-calibration technique. Note that the vertical axis of (b) is expanded by 200 times from that of (a). It is apparent that the fluctuations due to temperature change are drastically suppressed by use of the self-calibration technique. The variations in the measured film thicknesses of (b) are less than 0.11 nm.

## VI. CONCLUSION

A new prototype system of the CSE was developed to reduce the major systematic and random errors with the pre-

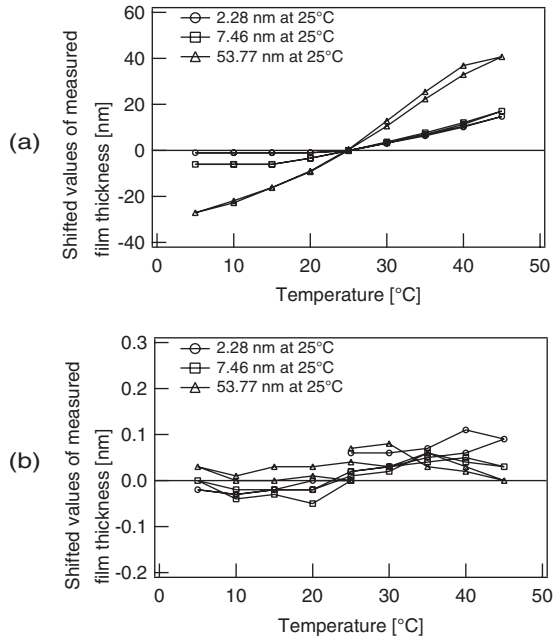


FIG. 10. Temperature-induced shifts in the measured thicknesses from the values at 25 °C. (a) and (b) respectively show the results obtained without and with the self-calibration technique. Note that the vertical axis of (b) is expanded by 200 times from that of (a).

Downloaded 15 Nov 2009 to 133.87.26.227. Redistribution subject to AIP license or copyright; see http://rsi.aip.org/rsi/copyright.jsp

vious CSEs. It was shown that the major causes of the systematic errors of the previous CSEs were the unbalanced Fresnel reflections of the high-order retarders and the bandwidth limitation during the demodulations of the ellipsometric parameters. Their influences can be eliminated or compensated for by changing the retarder thicknesses and the signal processing procedures. It was also explained that the major causes of the random errors of the previous CSEs are the mechanical stimulations to the fiber and the temperature variation of the high-order retarders, which degrade the stability and the repeatability. A fiber unit incorporating a diffuser is employed by the new CSE to reduce the fluctuation due to the fiber bending. The self-calibration technique modified for use with the CSE is also employed to improve the stability against the temperature change.

The effectiveness of the error reduction schemes used in the new CSE was experimentally demonstrated. The film thicknesses measured by the new CSE show good agreements with the ones by the RC-SE for the 12 $SiO_2$ films whose thicknesses are ranging approximately from 3 to 4000 nm. The stabilities against the fiber bending and temperature change were both less than 0.11 nm in the film-thickness measurement.

The prototype system has a simple and compact, namely, palm-size, sensing head and its acquisition time is 20 ms. In view of these features, the CSE is promising for various applications. It should be noted that the CSE is developed not to replace the existing spectroscopic ellipsometers; the CSE is still under development and can have its own limitations. Our objective in this work is to open up new applications of the spectroscopic ellipsometers in which the merits of the CSE, such as the compactness, the simplicity, and the rapid response, are essential. For example, the CSE should be useful for the in-line monitoring of the film thickness.

[1] T. Kato, K. Oka, S. Tanaka, and K. Ohtsuka, in *Extended Abstracts of the 34th Meeting of the Hokkaido Chapter of the Japan Society of Applied Physics* (The Hokkaido Chapter of the Japan Society of Applied Physics, Sapporo, 1998), p. 41 (in Japanese).
[2] K. Oka and T. Kato, Opt. Lett. **24**, 1475 (1999).
[3] R. W. Collins, Rev. Sci. Instrum. **61**, 2029 (1990).
[4] G. E. Jellison, Jr. and F. A. Modine, J. Appl. Phys. **53**, 3745 (1982).
[5] H. Okabe, K. Matoba, M. Hayakawa, A. Taniguchi, K. Oka, H. Naito, and N. Nakatsuka, Proc. SPIE **5878**, 58780H (2005).
[6] E. Kim, D. Dave, and T. E. Milner, Opt. Commun. **249**, 351 (2005).
[7] M. W. Kudenov, N. A. Hagen, E. L. Dereniak, and G. R. Gerhart, Opt. Express **15**, 12792 (2007).
[8] K. Oka and T. Kato, Proc. SPIE **4481**, 137 (2002).
[9] K. Oka and T. Kato, in Proceedings of 26th Meeting on Lightwave Sensing Technology, 2000 (unpublished), pp. 107–114 (in Japanese).
[10] H. Okabe, M. Hayakawa, K. Matoba, A. Taniguchi, K. Oka, and H. Naito, in Fouth International Conference on Spectroscopic Ellipsometry, 2007, edited by M. Schubert (unpublished), p. 173.
[11] Y. Yamamoto, J. Phys. (Paris) **44**, C10–35 (1983).
[12] H. Okabe, M. Hayakawa, H. Naito, A. Taniguchi, and K. Oka, Opt. Express **15**, 3093 (2007).
[13] *Handbook of Optical Constants of Solids III*, edited by E. D. Palic (Academic, San Diego, 1998).
[14] D. Sabatke, A. Locke, E. I. Dereniak, M. Descour, J. Garcia, T. Hamilton, and R. W. McMillan, Opt. Eng. (Bellingham) **41**, 1048 (2002).
[15] A. Taniguchi, K. Oka, H. Okabe, H. Naito, and N. Nakatsuka, Conference on Lasers and Electro-Optics/Quantum Electronics and Laser Science Conference and Photonic Applications Systems Technologies, Technical Digest (CD), 2006 (unpublished), Paper No. CTuV5.
[16] A. Taniguchi, K. Oka, H. Okabe, and M. Hayakawa, Opt. Lett. **31**, 3279 (2006).
[17] *Handbook of Optical Constants of Solids*, edited by E. D. Palic (Academic, San Diego, 1985).
[18] G. E. Jellison, Thin Solid Films **234**, 416 (1993).

**Downloaded 15 Nov 2009 to 133.87.26.227. Redistribution subject to AIP license or copyright; see http://rsi.aip.org/rsi/copyright.jsp**